Title
Uniform Diffusion of Cooper Pairing Mediated by Hole Carriers in Topological Sb2Te3/Nb

Journal
ACS Nano, 18(45)

ISSN
1936-0851

Authors
Hlevyack, Joseph A
Najafzadeh, Sahand
Li, Yao
et al.

Publication Date
2024-11-12

DOI
10.1021/acsnano.4c10533

Uniform Diffusion of Cooper Pairing Mediated by Hole Carriers in Topological Sb_2Te_3/Nb

Joseph A. Hlevyack[1,2]†, *Sahand Najafzadeh*[3]†, *Yao Li*[1,2], *Tsubaki Nagashima*[3], *Akifumi Mine*[3], *Yigui Zhong*[3], *Takeshi Suzuki*[3], *Akiko Fukushima*[3], *Meng-Kai Lin*[4], *Soorya Suresh Babu*[1,2], *Jinwoong Hwang*[5], *Ji-Eun Lee*[5], *Sung-Kwan Mo*[5], *James N. Eckstein*[1,2], *Shik Shin*[3,6]‡, *Kozo Okazaki*[3]*, *and Tai-Chang Chiang*[1,2]*

[1]Department of Physics, University of Illinois at Urbana-Champaign, Urbana, Illinois 61801, USA

[2]Frederick Seitz Materials Research Laboratory, University of Illinois at Urbana-Champaign, Urbana, Illinois 61801, USA

[3]Institute for Solid State Physics, The University of Tokyo, Kashiwa, Chiba 277-8581, Japan

[4]Department of Physics, National Central University, Taoyuan 32001, Taiwan

[5]Advanced Light Source, Lawrence Berkeley National Laboratory, Berkeley, California 94720, USA

[6]Office of University Professor, The University of Tokyo, Kashiwa, Chiba 277-8581, Japan

*Corresponding authors.

Email: tcchiang@illinois.edu (T.-C.C.); okazaki@issp.u-tokyo.ac.jp (K.O.)

†These authors contributed equally to this work.

‡This author is posthumously recognized.

ABSTRACT

Spin-helical Dirac fermions at a doped topological insulator's boundaries can support Majorana quasiparticles when coupled with *s*-wave superconductors, but in *n*-doped systems, the requisite induced Cooper pairing in topological states is often buried at heterointerfaces or complicated by degenerate coupling with bulk conduction carriers. Rarely probed are *p*-doped topological structures with nondegenerate Dirac and bulk valence bands at the Fermi level, which may foster long-range superconductivity without sacrificing Majorana physics. Using ultrahigh-resolution photoemission, we report proximity pairing with a large decay length in *p*-doped topological Sb_2Te_3 on superconducting Nb. Despite no momentum-space degeneracy, topological and bulk states of Sb_2Te_3/Nb exhibit the same isotropic superconducting gaps at low temperatures. Our results unify principles for realizing accessible pairing in Dirac fermions relevant to topological superconductivity.

KEYWORDS: Proximity effects, topological superconductivity, *p*-doped topological insulators, interband superconducting coherence, flip-chip method, thin-film heterostructures

Majorana zero modes in topological superconductors have enamored fundamental condensed-matter physics in recent years,[1–5] as their non-Abelian exchange statistics is conducive for building fault-tolerant qubits.[3,4] Nevertheless, an intrinsic topological superconductor with bulk spin-triplet superconductivity or an effective *p*-wave pairing state is quite rare,[4–9] especially since many candidates require delicate elemental alloying or are themselves highly contentious.[6–9] A more common contender for hosting Majorana bound states is a topological insulator coupled with an *s*-wave superconductor,[4,5,10–15] wherein an isotropic proximity-induced superconducting gap arises in the spin-helical Dirac fermions.[8–15] Such pairing can subsist at both boundaries of the topological insulator if Cooper pairs have sufficient phase coherence over large distances,[14–18] but mechanisms for mediating this robust superconductivity in the nontrivial boundary states remain fiercely debated.[14–21]

Fortunately, for heavily *n*-doped topological insulators on niobium with conduction band (CB) carriers, quantum-mechanical coupling between bulk and surface states rather simply fosters long-range proximity pairing.[15–18] Yet even this scenario does not necessarily apply to heavily *p*-doped topological insulators (Figure 1A,B). In *n*+ doped Bi_2Se_3, the Fermi level crosses the topological surface states (TSS) and CB, which nearly overlap in momentum space (Figure 1A).[15,22] Consequently, a large proximity-induced gap emerges in the TSS of Bi_2Se_3/Nb.[15–17] For bulk insulating *n* doped $(Bi_{1-x}Sb_x)_2Te_3$ with $x = 0.62$, the Fermi level lies in the bulk band gap, crossing the TSS above the Dirac point (Figure 1A).[18,23] No clear proximity pairing is observed here for $(Bi_{1-x}Sb_x)_2Te_3$/Nb, suggesting bulk CB are important for transiting pairing into the TSS.[15–18] Further increasing the alloy ratio x to $x = 1$ induces a Lifshitz transition to *p*+ doped Sb_2Te_3 (Figure 1A) with the Fermi level pinned to bulk valence bands (VB).[23–26] At this stage, the Fermi surface (Figure 1B) exhibits well-separated hole pockets due to the TSS and VB.[24,25] Thus, unlike Bi_2Se_3, Sb_2Te_3 is a clean topological material with bulk and surface states well separated in *k* space. This *k*-space separation can impact proximity pairing mediated by the bulk states,[15,18] but such intrinsic issues and proximity pairing overall in *p*-doped systems are rarely examined.[11–21]

Here, by conducting ultrahigh-resolution photoemission of heavily *p*-doped topological Sb_2Te_3 films on superconducting Nb, we find an isotropic superconducting gap opening within experimental error at low temperatures. Like bulk insulating $(Bi_{1-x}Sb_x)_2Te_3$/Nb, topological Sb_2Te_3/Nb is a simple system for stringently tuning quantum-mechanical interactions relevant to proximity effects:[15–18] The electronic structure of Sb_2Te_3 near the Fermi level has bulk and surface states at very different momenta (Figure 1B),[24–26] and bulk Nb has the highest transition temperature of all elemental *s*-wave superconductors ($T_{C,\,Nb} = 9.26$ K).[27–30] By fabricating Sb_2Te_3/Nb using our very own cleavage-based "flip-chip" method,[15,18] we create a topological material on Nb where hole-like Dirac and bulk VB bands do not overlap in momentum space at the Fermi level. Despite this separation, proximity-induced superconductivity quantified as a function of Sb_2Te_3 thickness reveals appreciable superconducting gaps of identical magnitude in the TSS and VB, implying that Cooper pairing is transferred from bulk VB to TSS through internal proximity effects mediated by interband superconducting coherence.[6–9] This discovery of *s*-wave superconductivity on Sb_2Te_3/Nb surfaces clarifies routes towards accessible pairing in the TSS, which could herald emergent physics, including topological superconductivity, in nanoscale devices.

RESULTS AND DISCUSSION

Confirming *p*-Type Doping and Fabricating Sb_2Te_3/Nb. High-quality, heavily *p*-doped Sb_2Te_3 films with thicknesses $N = 3$–7 quintuple layers (QL) (1 QL ≈ 1 nm) are grown using molecular beam epitaxy (MBE) onto bilayer-graphene-terminated SiC, as verified by *in situ* angle-resolved photoemission spectroscopy (ARPES) (Figures S1 and S2). Specifically, ARPES and second-derivative spectra along $\overline{\Gamma M}$ of as-grown 7 QL Sb_2Te_3 exhibit only the lower half of the topological Dirac cone and bulk VB located away from the zone center (Figure 1C).[23–26] Moreover, no bulk VB overlap with the TSS in momentum space at the Fermi level, even in bulk-like 7 QL Sb_2Te_3 (Figures 1C and S2). Corresponding Fermi surface maps of Sb_2Te_3 films also reveal typical band topologies for *p*-doped topological insulators:[24,25] A round contour centered at the $\bar{\Gamma}$ point due to the TSS and an elongated spoke along each $\overline{\Gamma M}$ from hole-like VB (Figure 1B,D). Evidently, all Sb_2Te_3 films are *p*-doped with bulk and surface bands crossing the Fermi level at very different momenta—quite unlike the nearly degenerate bulk CB and TSS of *n*+ doped Bi_2Se_3 in Figure 1A.[14,15,22]

All Sb_2Te_3/Nb films are fabricated using a "flip-chip" technique we invented for assembling van der Waals materials onto arbitrary superconductors,[15] which sidesteps mixed interfacial structures and Nb diffusion encountered when growing topological films on Nb.[19,31] After MBE growths of Sb_2Te_3 films on bilayer-graphene-terminated SiC, a 60-nm-thick bulk Nb film is deposited atop using magnetron sputtering at 25 °C (Figure 1E, step 1). Each sample is then flipped over, attached to a polished Cu plate by an electrically conductive epoxy, and finally capped with a cleavage pin (Figure 1E, steps 2 and 3). Just prior to photoemission, each thin-film structure is cleaved *in situ* by pushing against the cleavage pin (Figure 1E, step 4) to separate the substrate held in place by weak incommensurate van der Waals bonding, yielding Sb_2Te_3 films with thicknesses set by MBE on superconducting Nb.[15,18] Large, mirrorlike Sb_2Te_3/Nb surfaces perfect for ARPES are easily obtainable with this flip-chip method (Figures S3 and S4).

Pairing in Bulk and Topological Bands of Flip-Chip Sb_2Te_3/Nb. Ultrahigh-resolution photoemission measurements are undertaken with *p*-polarized 5.821-eV and/or 6.994-eV photons at temperatures $T = 1.5$–10 K. Typical constant energy contours near the Fermi level at $T < 2$ K for Sb_2Te_3/Nb are presented in Figure 2A–C. A representative dataset for proximity pairing in Sb_2Te_3/Nb—one with constant energy contours, temperature-dependent band maps of the TSS and VB close to the Fermi level, and energy distribution curves (EDCs) at strategically chosen Fermi surface momenta—is summarized for the 4 QL case in Figure 2C– E. Like the

Fermi surface map of its as-grown counterpart (Figure 1D), constant energy contour maps at 6.994-eV and 5.821-eV photon energies for 7 QL Sb_2Te_3/Nb each possess a zone-centered, hooplike contour and an intensity arm along $\overline{\Gamma M}$ due to the hole-like TSS and VB, respectively (Figure 2A).[24,25] Similar statements are duly noted for the constant energy contour maps of 3 QL and 4 QL flip chips (Figure 2B,C), though the density of bulk-like VB near the Fermi level in the 3 QL case is reduced due to quantum-size effects (Figure S2).[22,32,33] Incidentally, all these constant energy contours flaunt complex variations in photoemission intensity as a function of photon energy and/or in-plane momenta (Figure 2A–C), attributable to matrix element effects tied to the surface's orientation relative to the incident photon beam's electric field.[32]

Quintessential features of proximity pairing at temperatures below the superconducting transition temperature of bulk Nb arise in temperature-dependent band maps of 4 QL Sb_2Te_3/Nb (Figure 2D). Namely, band mappings of TSS and VB features exhibit thermally broadened Fermi-level cutoffs at $T = 10$ K, but as the temperature is reduced to $T = 1.8$ K, superconducting coherence peaks and associated leading-edge shifts emerge at all in-plane momenta (Figure 2D), indicative of induced superconducting order in both the TSS and VB. The development of a coherence peak at momenta other than the Fermi momenta is due to quasiparticle interference augmented by superconducting phase coherence.[6–9] Despite their differences in Fermi momentum along $\overline{\Gamma M}$ (k_y-direction) (Figure 2C), all EDC datasets in Figure 2E show virtually identical temperature-dependent leading-edge shifts and thus proximity-induced gaps, which we quantify by modelling superconducting EDCs with Gaussian-broadened Dynes functions having Fermi-level cutoffs and BCS mean-field dependencies for the superconducting gaps (Figure 2E, blue curves). That is, the superconducting Dynes density of states (DOS) at binding energy E_B

with pair-breaking parameter Γ and superconducting gap $\Delta = \Delta(T)$ is

$$N_S(E_B, \Gamma, \Delta) = \mathrm{Re}\left(\frac{|E_B + i\Gamma|}{\sqrt{(E_B + i\Gamma)^2 - \Delta^2}}\right), \quad (1)$$

where $\Delta = \Delta(0)\tanh\left(1.74\sqrt{T_C/T - 1}\right)$.[7,15,34] Here, the zero-temperature gap Δ(0) is a universal fitting parameter in the analysis of each temperature-dependent EDC dataset (Figures 2E, 3, and 4), while T_C is the transition temperature of flip-chip Sb_2Te_3/Nb, which is within experimental error equivalent to that of bulk Nb as determined from transport of 60-nm-thick Nb film (Figure S5).[27–30] The agreement between raw EDCs and their corresponding fits is excellent for 4 QL Sb_2Te_3/Nb and overall suggests that the TSS and VB have similar superconducting gaps, evocative of an isotropic gap in the 4 QL Sb_2Te_3/Nb Fermi surface (Figure 2C–E). However, these conclusions apply equally well to other N QL Sb_2Te_3/Nb, as shown by their fitted topological and bulk EDCs in Figure 3. Meanwhile, as the thickness of N QL Sb_2Te_3/Nb increases from $N = 0$ to 7, superconductivity at the surface exhibits a characteristic decay with obvious superconducting features no longer visible in 7 QL Sb_2Te_3/Nb (Figure 3), all reflective of the expected phase decoherence of Cooper pairs with increasing distance away from the superconducting heterointerface.[14–21,35]

Momentum-Resolved Zero-Temperature Gaps in Sb_2Te_3/Nb. To more explicitly highlight the isotropic nature of the proximity gap, Figure 4A plots all deduced zero-temperature gaps Δ(0) versus Sb_2Te_3 film thickness, while Figure 4B displays these same thickness-dependent Δ(0) but now resolved as a function of in-plane momenta along $\overline{\Gamma \mathrm{K}}$ (k_x-direction) and $\overline{\Gamma \mathrm{M}}$ (k_y-direction) of Sb_2Te_3/Nb. Clearly, for a given Sb_2Te_3 thickness, the induced gap is the same across the Fermi surface, indicative of an isotropic s-wave gap (Figure 4A,B). In line with thickness-dependent EDCs in Figure 3, $\Delta(0)$ decreases with increasing Sb_2Te_3 film thickness so that at a 7 QL thickness, only a small superconducting gap is inferred (Figure 4A). Furthermore, the decay length λ of Cooper pairs penetrating into an Sb_2Te_3 film of thickness z may be estimated by fitting the thickness dependence of $\Delta(0)$ with an exponential function (Figure 4A, blue curve) given by

$$\Delta(0) = \Delta_0 \exp\left(-\frac{z}{\lambda}\right), \tag{2}$$

where $\Delta_0 = 1.591$ meV is the zero-temperature superconducting gap of Nb found from simultaneous fitting of pure Nb data (Figure 3, top panel). The extracted decay length is $\lambda = 4.668 \pm 0.003$ QL. Also, by suggestion of the thickness-dependent behavior of $\Delta(0)$, a linear fit (Figure 4A, red curve) gives a lower bound estimate for $\Delta(0)$ in the 7 QL system, which is comparable to the analyzer's maximum energy resolution (~0.1 meV).[15,36–38] Overall, our results demonstrate the opening of an isotropic *s*-wave gap in all Sb_2Te_3/Nb Fermi surfaces and therefore that the TSS and VB—located at different momenta at the Fermi level—possess comparable zero-temperature gaps (Figures 3 and 4).

CONCLUSIONS

Fundamental to realizing long-range induced pairing in doped topological insulators on Nb is the presence of bulk VB or CB carriers (Figures 1A and 2), but the Fermi surface topology of *p*-doped Sb_2Te_3—namely, hole-like TSS and VB well separated in momentum space (Figure 1D)—and its role in channeling or hindering this superconductivity have been overlooked.[15,18] Cooper pairing induced into Sb_2Te_3 via Andreev reflection at the heterointerface is transported to the Sb_2Te_3 surface through bulk VB hole carriers since unlike topological quasiparticles, their wavefunctions are spatially distributed throughout Sb_2Te_3 (Figures S6–

S9).[32,33] Naturally, such Cooper pairs lose their phase coherence at large distances away from the Sb_2Te_3/Nb heterojunction as the proximity-induced gap decays with increasing Sb_2Te_3 thickness (Figures 3 and 4).[15–18,35] Upon reaching the surface through VB carriers, Cooper pairing is transmitted into the TSS through internal proximity effects imposed by interband superconducting coherence in momentum space,[6–9] because the TSS are localized within the first couple QL (Figures S6–S9) and cannot couple effectively with Cooper pairs at the Sb_2Te_3/Nb interface. This coherence is also inherited from the underlying Nb, which manifests an *s*-wave superconducting gap across its Fermi surface at low temperatures.[7,39,40]

Thus, while hole-like bulk VB in *p*-doped Sb_2Te_3/Nb are pure channels nondegenerate with TSS at the Fermi level, they are nevertheless arbitrators of self-induced proximity effects that impress isotropic *s*-wave gaps onto the TSS.[6–9] This situation contrasts from that of *n*-doped Bi_2Se_3/Nb, where the TSS and bulk CB are nearly degenerate at the Fermi level, which evidently enhances quantum-mechanical coupling and thus sharing of superconductivity between these states.[15,18] Incidentally, per Figure 4A, the quasiparticle coherence length of Cooper pairs in Sb_2Te_3/Nb (~4.7 QL) is also smaller than that of Bi_2Se_3/Nb (~8.4 QL);[15] the difference is attributable to coherent band structure mismatch of the doped topological insulator with Nb,[39,40] whose Fermi surface possesses multiple zone-centered bulk pockets—like Bi_2Se_3 but unlike the spatially localized TSS contour of Sb_2Te_3 (Figure 1B).[22,25] Lastly, since an *s*-wave gap arises in the spin-helical TSS (Figures 2–4), Sb_2Te_3 as a topological metal on Nb could host Majorana zero modes due to its Fermi surface topology of nondegenerate surface and bulk contours (Figure 2A–C),[8–10,16] but trivial VB carriers may obscure transport properties of these topological effects.[13,18,23,26] Overall, for doped topological insulators on Nb, if there are prominent bulk states at the Fermi level—even those separated in momentum space from the TSS, a long-range and isotropic superconducting gap will emerge on topological surfaces at low temperatures. Our findings add greater engineering flexibility for realizing robust pairing in nontrivial boundary states of artificial topological structures, which should guide searches for emergent quasiparticle excitations needed for building topological qubits.

METHODS

Fabrication of Sb_2Te_3/Nb. Before MBE growths of Sb_2Te_3 thin films at the University of Illinois, 6*H*-SiC(0001) substrates were degassed at ~500 °C for an hour and then annealed repeatedly to ~1300 °C, yielding bilayer-graphene-terminated surfaces. Afterwards, high-purity Sb and Te were co-evaporated from an electron-beam evaporator (Sb) and an effusion cell (Te) onto substrates heated to 280 °C. The Te/Sb flux ratio was 10:1, and the growth rate was typically ~15 min per QL. Subsequently, Sb_2Te_3 films were annealed at 310 °C for ~30 min to obtain smoother surfaces, as demonstrated by *in situ* reflection high-energy electron diffraction (RHEED) and photoemission. To fashion Sb_2Te_3/Nb flip chips, all Sb_2Te_3 films were coated with a 60-nm-thick polycrystalline (110)-oriented Nb film by magnetron sputtering at an Ar gas pressure of 6 mTorr and a power of 140–150 W; this deposition was done at ~25 °C to inhibit interdiffusion of Nb into Sb_2Te_3.[15,19,31] Each sample was then flipped over and glued onto a polished Cu plate with a low-temperature-curing Ag epoxy; a cleavage pin was lastly attached to the substrate's backside using similar epoxy.

Photoemission Measurements. Ultrahigh-resolution ARPES was performed at the Institute for Solid State Physics at The University of Tokyo in a laser-based setup, which consists of vacuum ultraviolet lasers with photon energies 6.994 eV and 5.821 eV, a Scienta HR8000 analyzer, and a sample manipulator cooled with superfluid liquid helium. Each Sb_2Te_3/Nb was crystallographically aligned onto the sample holder *ex situ* before cleavage based on the SiC substrate's high-symmetry cleavage planes and also the as-grown film's ARPES and RHEED measurements. Here, the geometry chosen had the momentum axis of each laser-ARPES map nominally parallel to $\overline{\Gamma K}$ (k_x-direction). Any sample misalignment was minimal per constant energy contour mappings of flip chips after cleavage (Figure 2). During laser-ARPES, the sample's temperature was tuned from 10 K down to 1.5 K, and the energy resolutions were ~1.6 meV and ~0.8 meV (or better) for 6.994-eV and 5.821-eV lasers, respectively. All Sb_2Te_3/Nb EDCs, from which BCS zero-temperature gaps were determined via eq 1, were acquired by integrating the ARPES intensity within ±0.015 Å^{-1} of the indicated momentum component k_x along $\overline{\Gamma K}$. For details about the Fermi-level calibration and simultaneous fittings of zero-temperature gaps (Figures S10 and S11), see the discussion in the Supporting Information and methods in prior works.[15,18,36–38] ARPES maps of as-grown Sb_2Te_3 were garnered at the University of Illinois at 30 K using a Scienta-Omicron VUV5k He lamp (21.22-eV photons) and a Scienta R4000 analyzer. Preliminary ARPES data to validate the flip-chip methodology were obtained at Beamline 10.0.1.1 (HERS) at the Advanced Light Source, Lawrence Berkeley National Laboratory.

Computational Details. First-principles calculations of freestanding Sb_2Te_3 films (Figures S6–S9) were conducted in the Quantum Espresso package[41] under the generalized gradient approximation with Perdew-Burke-Ernzerhof functionals.[42] Spin-orbit coupling was included. Projected augmented wave pseudopotentials with an energy cutoff of 612 eV were employed,[43] and a periodic slab geometry with a vacuum gap larger than 15 Å was adopted in the modeling of each Sb_2Te_3 film. The lattice constants of N QL Sb_2Te_3 for $N > 3$ were set to the bulk values ($a = 4.26$ Å and $c = 30.46$ Å),[26] while 3 QL Sb_2Te_3 was allowed to relax via Grimme dft-D3 corrections[44] with residual atomic forces less than 1 meV/Å. Band structure calculations were performed on Γ-centered $12 \times 12 \times 1$ Monkhorst-Pack grids[45] with the self-consistent convergence criterion for the total ground-state energy set to 10^{-7} eV.

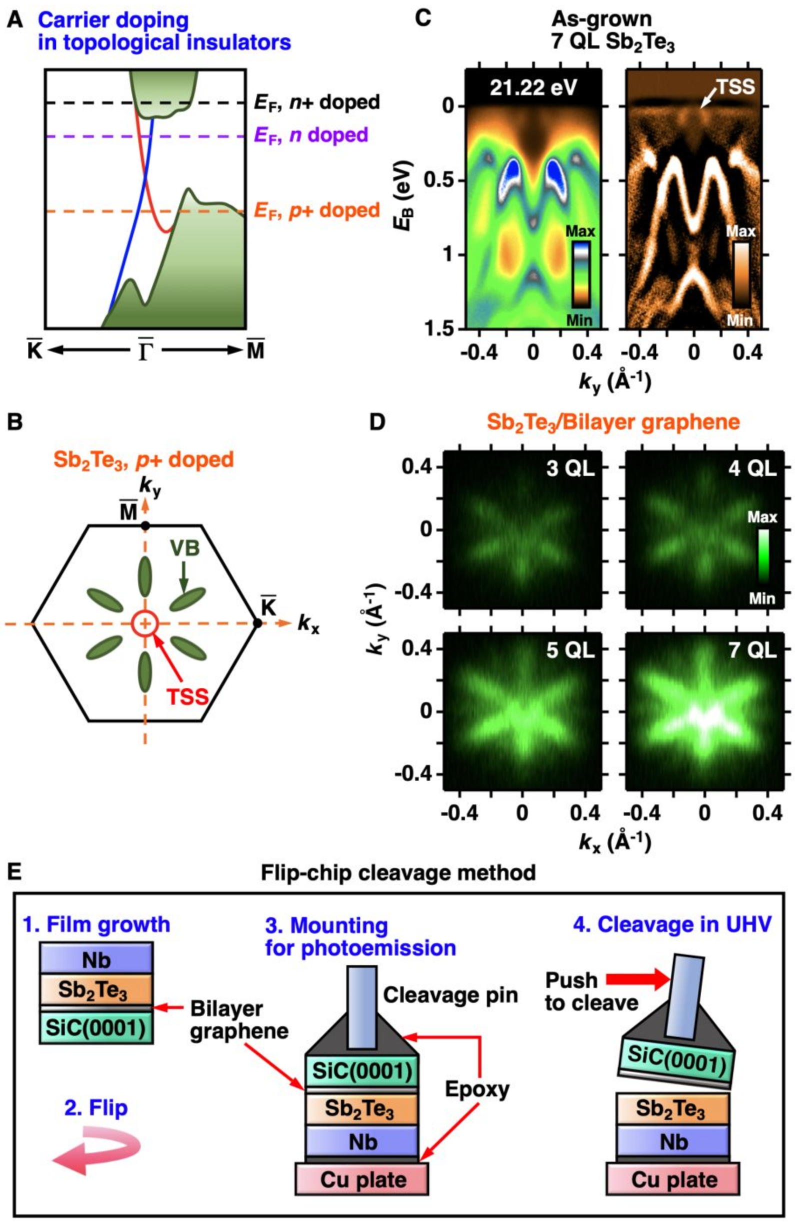

Figure 1. Fabricating p+ doped Sb_2Te_3 for Nb-based flip chips. (**A**) Schematic band structure of bulk carrier doping in topological insulators; dashed lines indicate Fermi levels for n+ (black), lightly n (purple), and p+ (orange) doped systems. (**B**) Sketch of the Fermi surface of Sb_2Te_3, which consists of elongated VB hole pockets (green) and a zone-centered TSS contour (red). (**C**) Photoemission spectra (left) and its two-dimensional second derivative (right) of as-grown 7 QL Sb_2Te_3 on bilayer graphene measured at 30 K along $\overline{\Gamma M}$ using 21.22-eV photons.

(**D**) Fermi surface maps of Sb_2Te_3 films taken at 30 K with 21.22-eV photons; to obtain each mapping, the ARPES intensity was integrated within ±10 meV of the Fermi level. (**E**) Diagram summarizing our flip-chip method for fabricating Sb_2Te_3 films on Nb.

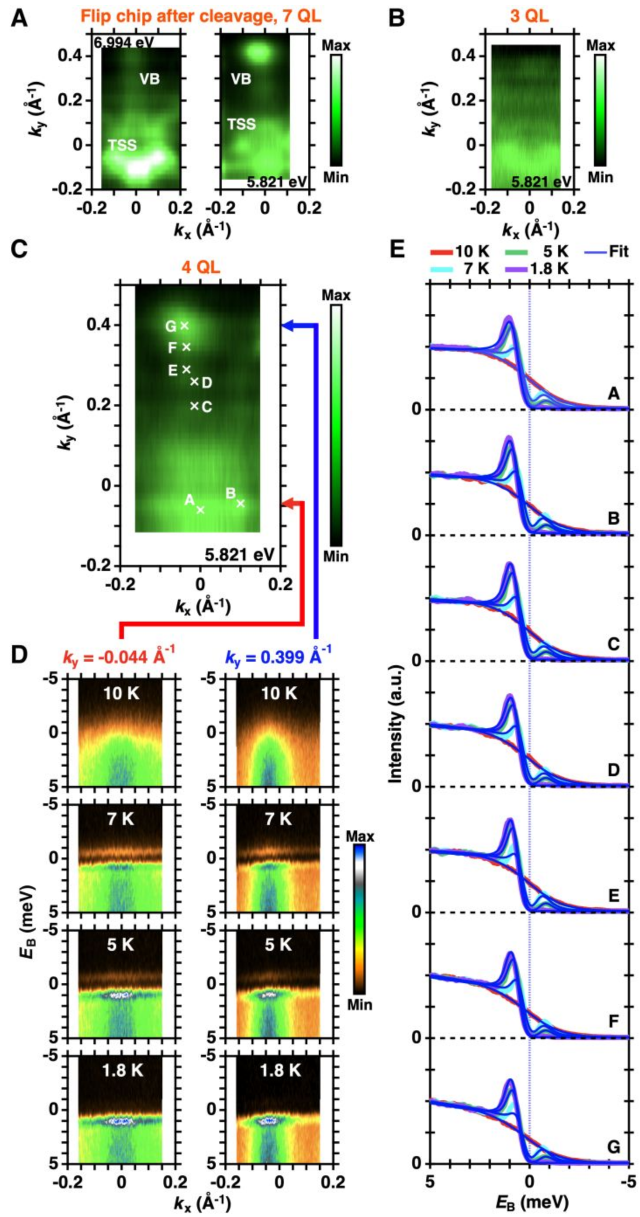

Figure 2. Constant energy contours and pairing in topological Sb_2Te_3/Nb. (**A**) Constant energy contours near the Fermi level of flip-chip 7 QL Sb_2Te_3/Nb after cleavage obtained with 6.994-eV (left) and 5.821-eV (right) photons at 1.8 K; contours due to VB and TSS are indicated in both maps, and to generate each map, the ARPES intensity was integrated from $E_B = 0$ to 5 meV. (**B**) Similar to (A) but for 3 QL Sb_2Te_3/Nb at 1.5 K. (**C**) Same as (B) but for 4 QL Sb_2Te_3/Nb at 1.8 K. (**D**) Select band maps at momentum cuts k_y along $\overline{\Gamma M}$ through the TSS (left)

and VB (right) identified by the connecting red and blue arrows to (C), respectively. (**E**) Temperature-dependent EDCs overlaid with BCS fits (blue curves) at momenta A–G labelled in (C).

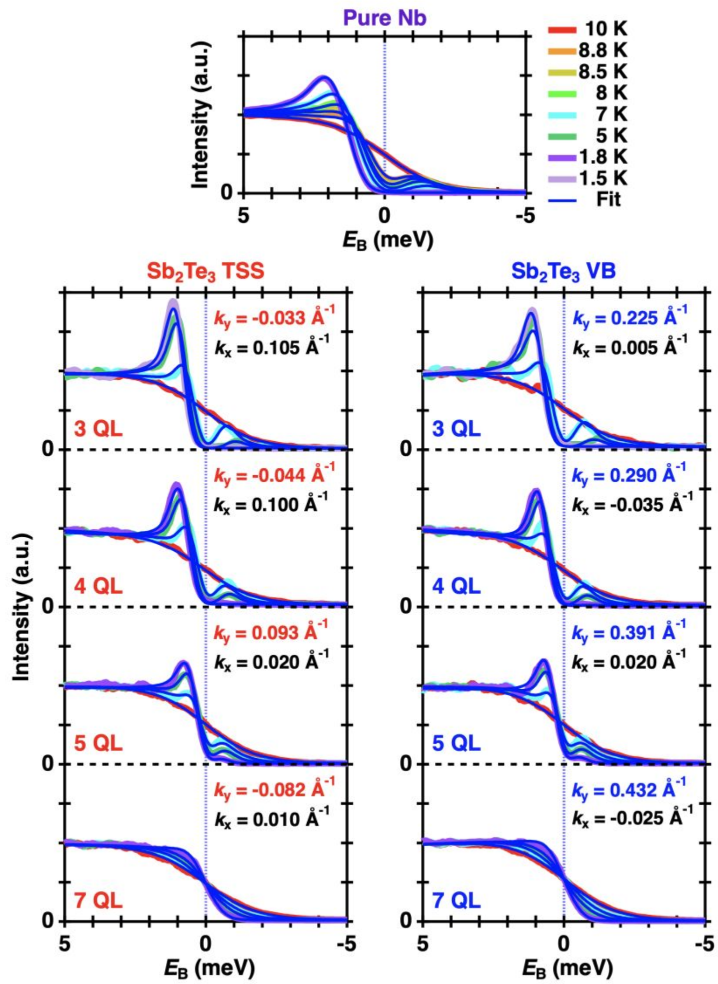

Figure 3. Bulk versus topological EDCs as a function of Sb_2Te_3 thickness. Results are reported for a pure Nb reference (top, 6.994-eV photons) and 3–7 QL Sb_2Te_3/Nb (bottom, 5.821-eV photons), and the blue curves in each panel are BCS fits. For every Sb_2Te_3/Nb EDC, the momentum components parallel to $\overline{\Gamma \mathrm{K}}$ (k_x-direction) and $\overline{\Gamma \mathrm{M}}$ (k_y-direction) are indicated.

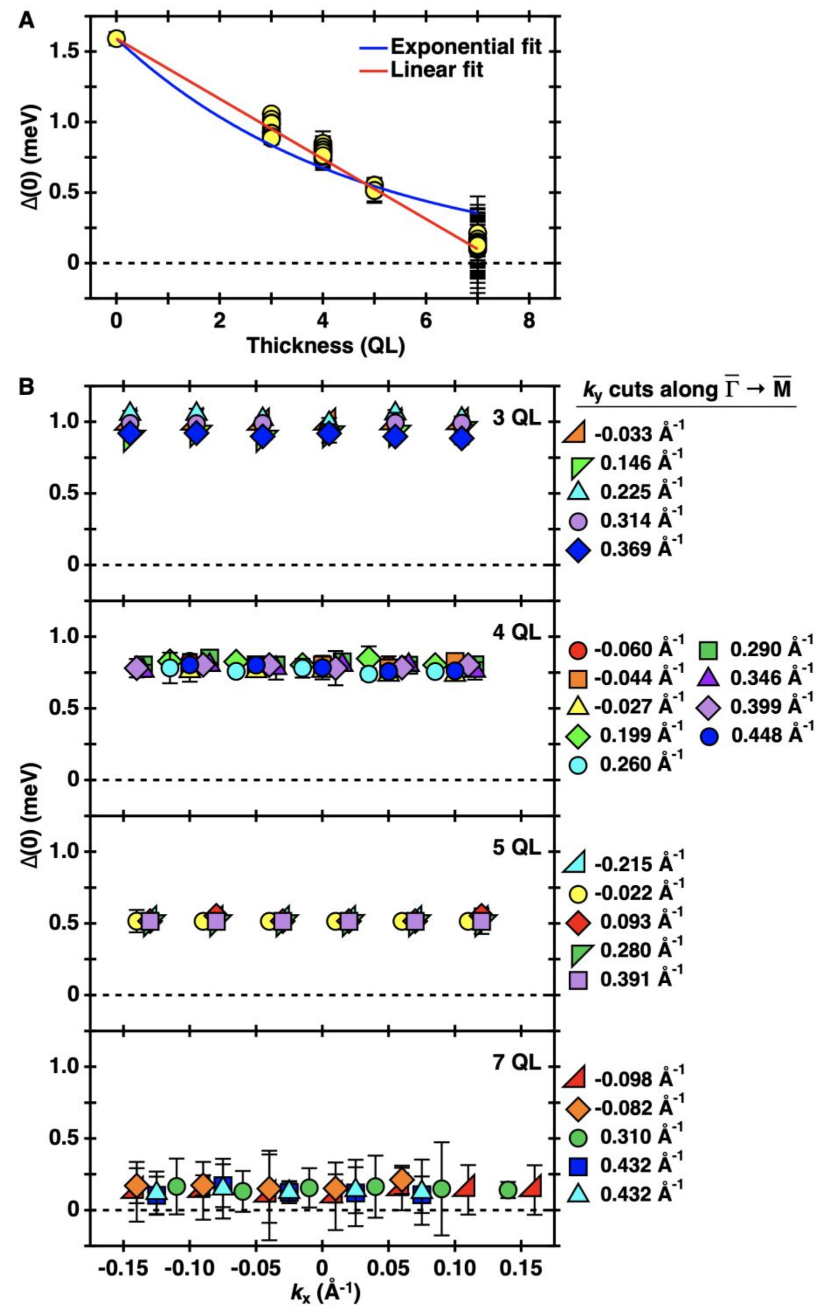

Figure 4. Momentum-resolved zero-temperature superconducting gaps versus thickness. (**A**) Zero-temperature gap Δ(0) versus Sb_2Te_3 film thickness overlaid with exponential (blue) and linear (red) fits. (**B**) Δ(0) as a function of Sb_2Te_3 film thickness and in-plane momenta along $\overline{\Gamma K}$ (k_x-direction) and $\overline{\Gamma M}$ (k_y-direction). The error bar for each gap is the standard deviation estimated by each simultaneous fit.

AUTHOR INFORMATION

Author Contributions. J.A.H. and T-C.C. conceived the project. J.A.H., Y.L., M.-K.L., and T.-C.C., with the aid of S.S.B. and J.N.E., conducted the MBE growths and with S.N., K.O., J.H., J.-E.L., and S.-K.M. designed and/or prepared flip-chip samples. S.N. and K.O., with the assistance of T.N., A.M., Y.Z., T.S., A.F., and S.S., performed the laser-ARPES measurements. Y.L. conducted the first-principles calculations. S.S.B. with J.N.E. performed the transport measurements. J.A.H., Y.L., M.-K.L., and T.-C.C., with feedback from J.H., J.-E.L., and S.-K.M., conducted ARPES characterizations at the University of Illinois. J.A.H., S.N., Y.L., T.N., A.M., M.-K.L., K.O., and T.-C.C. analyzed the data. T.-C.C., K.O., J.A.H., and S.N. interpreted the data. T.-C.C. led the group at the University of Illinois; K.O. led the group at the Institute for Solid State Physics. T.-C.C. organized the project.

Funding Sources

1. U.S. Department of Energy (DOE), Office of Science (OS), Office of Basic Energy Sciences, Division of Materials Science and Engineering, under Grant No. DE-FG02-07ER46383.
2. Grants-in-Aid for Scientific Research (KAKENHI) (Grant Nos. JP19H01818, JP19H00659, JP19H00651, JP24K01375, JP24K00565, and JP24KF0021) from the Japan Society for the Promotion of Science (JSPS).
3. JSPS KAKENHI on Innovative Areas “Quantum Liquid Crystals” (Grant No. JP19H05826).
4. Quantum Leap Flagship Program (Q-LEAP) (Grant No. JPMXS0118068681) from the Ministry of Education, Culture, Sports, Science, and Technology (MEXT).
5. National Science and Technology Council of Taiwan under Grant Nos. 110-2112-M-008-039-MY3 and 113-2112-M-008-035-MY3.

6. DOE Office of Science User Facility supported under Contract No. DE-AC02-05CH11231.

ACKNOWLEDGMENTS

This work was supported by the U.S. Department of Energy (DOE), Office of Science (OS), Office of Basic Energy Sciences, Division of Materials Science and Engineering, under Grant No. DE-FG02-07ER46383 (T.-C.C.), and by Grants-in-Aid for Scientific Research (KAKENHI) (Grant Nos. JP19H01818, JP19H00659, JP19H00651, JP24K01375, JP24K00565, and JP24KF0021) from the Japan Society for the Promotion of Science (JSPS), JSPS KAKENHI on Innovative Areas "Quantum Liquid Crystals" (Grant No. JP19H05826), and the Quantum Leap Flagship Program (Q-LEAP) (Grant No. JPMXS0118068681) from the Ministry of Education, Culture, Sports, Science, and Technology (MEXT) (K.O.). M.-K.L. acknowledges support from the National Science and Technology Council of Taiwan under Grant Nos. 110-2112-M-008-039-MY3 and 113-2112-M-008-035-MY3. We recognize that this work was partly carried out in the Central Research Facilities at the Frederick Seitz Materials Research Laboratory, University of Illinois at Urbana-Champaign. This research also used resources of the Advanced Light Source, which is a DOE Office of Science User Facility supported under Contract No. DE-AC02-05CH11231.

ABBREVIATIONS

CB, conduction band(s); TSS, topological surface state(s); VB, valence band(s); QL, quintuple layer(s); MBE, molecular beam epitaxy; ARPES, angle-resolved photoemission spectroscopy; EDC, energy distribution curve; DOS, density of states; RHEED, reflection high-energy electron diffraction

ASSOCIATED CONTENT

Supporting Information. Photoemission VB Mappings of As-Grown Films and Sb_2Te_3/Nb; Transport Measurements of Bulk Nb Resistance; First-Principles Computations for Freestanding Sb_2Te_3; Methods for Determining the Fermi Level and BCS Gap; Supporting References.

REFERENCES

1. Ivanov, D. A. Non-Abelian Statistics of Half-Quantum Vortices in *p*-Wave Superconductors. *Phys. Rev. Lett.* **2001**, *86* (2), 268–271. DOI: 10.1103/PhysRevLett.86.268
2. Qi, X.-L.; Hughes, T. L.; Raghu, S.; Zhang, S.-C. Time-Reversal-Invariant Topological Superconductors and Superfluids in Two and Three Dimensions. *Phys. Rev. Lett.* **2009**, *102* (18), No. 187001. DOI: 10.1103/PhysRevLett.102.187001
3. Kitaev, A. Y. Fault-Tolerant Quantum Computation by Anyons. *Ann. Phys. (N. Y.)* **2003**, *303* (1), 2–30. DOI: 10.1016/S0003-4916(02)00018-0
4. Alicea, J. New Directions in the Pursuit of Majorana Fermions in Solid State Systems. *Rep. Prog. Phys.* **2012**, *75* (7), No. 076501. DOI: 10.1088/0034-4885/75/7/076501
5. Frolov, S. M.; Manfra, M. J.; Sau, J. D. Topological Superconductivity in Hybrid Devices. *Nat. Phys.* **2020**, *16* (7), 718–724. DOI: 10.1038/s41567-020-0925-6
6. Chang, T.-R.; Chen, P.-J.; Bian, G.; Huang, S.-M.; Zheng, H.; Neupert, T.; Sankar, R.; Xu, S.-Y.; Belopolski, I.; Chang, G.; Wang, B.; Chou, F.; Bansil, A.; Jeng, H.-T.; Lin, H.; Hasan, M. Z. Topological Dirac Surface States and Superconducting Pairing Correlations in $PbTaSe_2$. *Phys. Rev. B* **2016**, *93* (24), No. 245130. DOI: 10.1103/PhysRevB.93.245130

7. Guan, S.-Y.; Chen, P.-J.; Chu, M.-W.; Sankar, R.; Chou, F.; Jeng, H.-T.; Chang, C.-S.; Chuang, T.-M. Superconducting Topological Surface States in the Noncentrosymmetric Bulk Superconductor $PbTaSe_2$. *Sci. Adv.* **2016**, *2* (11), No. e1600894. DOI: 10.1126/sciadv.1600894

8. Zhang, P.; Yaji, K.; Hashimoto, T.; Ota, Y.; Kondo, T.; Okazaki, K.; Wang, Z.; Wen, J.; Gu, G. D.; Ding, H.; Shin, S. Observation of Topological Superconductivity on the Surface of an Iron-Based Superconductor. *Science* **2018**, *360* (6385), 182–186. DOI: 10.1126/science.aan4596

9. Li, Y. W.; Zheng, H. J.; Fang, Y. Q.; Zhang, D. Q.; Chen, Y. J.; Chen, C.; Liang, A. J.; Shi, W. J.; Pei, D.; Xu, L. X.; Liu, S.; Pan, J.; Lu, D. H.; Hashimoto, M.; Barinov, A.; Jung, S. W.; Cacho, C.; Wang, M. X.; He, Y.; Fu, L.; *et al.* Observation of Topological Superconductivity in a Stoichiometric Transition Metal Dichalcogenide 2M-WS_2. *Nat. Commun.* **2021**, *12* (1), No. 2874. DOI: 10.1038/s41467-021-23076-1

10. Fu, L.; Kane, C. L. Superconducting Proximity Effect and Majorana Fermions at the Surface of a Topological Insulator. *Phys. Rev. Lett.* **2008**, *100* (9), No. 096407. DOI: 10.1103/PhysRevLett.100.096407

11. Zhu, Z.; Papaj, M.; Nie, X.-A.; Xu, H.-K.; Gu, Y.-S.; Yang, X.; Guan, D.; Wang, S.; Li, Y.; Liu, C.; Luo, J.; Xu, Z.-A.; Zheng, H.; Fu, L.; Jia, J.-F. Discovery of Segmented Fermi Surface Induced by Cooper Pair Momentum. *Science* **2021**, *374* (6573), 1381–1385. DOI: 10.1126/science.abf1077

12. Yi, H.; Hu, L.-H.; Wang, Y.; Xiao, R.; Cai, J.; Reifsnyder Hickey, D.; Dong, C.; Zhao, Y.-F.; Zhou, L.-J.; Zhang, R.; Richardella, A. R.; Alem, N.; Robinson, J. A.; Chan, M. H. W.; Xu, X.; Samarth, N.; Liu, C.-X.; Chang, C.-Z. Crossover from Ising- to Rashba-Type

Superconductivity in Epitaxial Bi_2Se_3/Monolayer $NbSe_2$ Heterostructures. *Nat. Mater.* **2022**, *21* (12), 1366–1372. DOI: 10.1038/s41563-022-01386-z

13. Li, C.; Zhao, Y.-F.; Vera, A.; Lesser, O.; Yi, H.; Kumari, S.; Yan, Z.; Dong, C.; Bowen, T.; Wang, K.; Wang, H.; Thompson, J. L.; Watanabe, K.; Taniguchi, T.; Reifsnyder Hickey, D.; Oreg, Y.; Robinson, J. A.; Chang, C.-Z.; Zhu, J. Proximity-Induced Superconductivity in Epitaxial Topological Insulator/Graphene/Gallium Heterostructures. *Nat. Mater.* **2023**, *22* (5), 570–575. DOI: 10.1038/s41563-023-01478-4
14. Xu, S.-Y.; Alidoust, N.; Belopolski, I.; Richardella, A.; Liu, C.; Neupane, M.; Bian, G.; Huang, S.-H.; Sankar, R.; Fang, C.; Dellabetta, B.; Dai, W.; Li, Q.; Gilbert, M. J.; Chou, F.; Samarth, N.; Hasan, M. Z. Momentum-Space Imaging of Cooper Pairing in a Half-Dirac-Gas Topological Superconductor. *Nat. Phys.* **2014**, *10* (12), 943–950. DOI: 10.1038/nphys3139
15. Flötotto, D.; Ota, Y.; Bai, Y.; Zhang, C.; Okazaki, K.; Tsuzuki, A.; Hashimoto, T.; Eckstein, J. N.; Shin, S.; Chiang, T.-C. Superconducting Pairing of Topological Surface States in Bismuth Selenide Films on Niobium. *Sci. Adv.* **2018**, *4* (4), No. eaar7214. DOI: 10.1126/sciadv.aar7214
16. Lee, K.; Vaezi, A.; Fischer, M. H.; Kim, E.-A. Superconducting Proximity Effect in Topological Metals. *Phys. Rev. B* **2014**, *90* (21), No. 214510. DOI: 10.1103/PhysRevB.90.214510
17. Park, K.; Csire, G.; Ujfalussy, B. Proximity Effect in a Superconductor-Topological Insulator Heterostructure Based on First Principles. *Phys. Rev. B* **2020**, *102* (13), No. 134504. DOI: 10.1103/PhysRevB.102.134504
18. Hlevyack, J. A.; Najafzadeh, S.; Lin, M.-K.; Hashimoto, T.; Nagashima, T.; Tsuzuki, A.; Fukushima, A.; Bareille, C.; Bai, Y.; Chen, P.; Liu, R.-Y.; Li, Y.; Flötotto, D.; Avila, J.;

Eckstein, J. N.; Shin, S.; Okazaki, K.; Chiang, T.-C. Massive Suppression of Proximity Pairing in Topological $(Bi_{1-x}Sb_x)_2Te_3$ Films on Niobium. *Phys. Rev. Lett.* **2020**, *124* (23), No. 236402. DOI: 10.1103/PhysRevLett.124.236402

19. Zang, Y.; Küster, F.; Zhang, J.; Liu, D.; Pal, B.; Deniz, H.; Sessi, P.; Gilbert, M. J.; Parkin, S. S. P. Competing Energy Scales in Topological Superconducting Heterostructures. *Nano Lett.* **2021**, *21* (7), 2758–2765. DOI: 10.1021/acs.nanolett.0c04648
20. Zhao, H.; Rachmilowitz, B.; Ren, Z.; Han, R.; Schneeloch, J.; Zhong, R.; Gu, G.; Wang, Z.; Zeljkovic, I. Superconducting Proximity Effect in a Topological Insulator Using Fe(Te, Se). *Phys. Rev. B* **2018**, *97* (22), No. 224504. DOI: 10.1103/PhysRevB.97.224504
21. Qin, H.; Guo, B.; Wang, L.; Zhang, M.; Xu, B.; Shi, K.; Pan, T.; Zhou, L.; Chen, J.; Qiu, Y.; Xi, B.; Sou, I. K.; Yu, D.; Chen, W.-Q.; He, H.; Ye, F.; Mei, J.-W.; Wang, G. Superconductivity in Single-Quintuple-Layer Bi_2Te_3 Grown on Epitaxial FeTe. *Nano Lett.* **2020**, *20* (5), 3160–3168. DOI: 10.1021/acs.nanolett.9b05167
22. Liu, J.; Yang, X.; Xue, H.; Gai, X.; Sun, R.; Li, Y.; Gong, Z.-Z.; Li, N.; Xie, Z.-K.; He, W.; Zhang, X.-Q.; Xue, D.; Cheng, Z.-H. Surface Coupling in Bi_2Se_3 Ultrathin Films by Screened Coulomb Interaction. *Nat. Commun.* **2023**, *14* (1), No. 4424. DOI: 10.1038/s41467-023-40035-0
23. Zhang, J.; Chang, C.-Z.; Zhang, Z.; Wen, J.; Feng, X.; Li, K.; Liu, M.; He, K.; Wang, L.; Chen, X.; Xue, Q.-K.; Ma, X.; Wang, Y. Band Structure Engineering in $(Bi_{1-x}Sb_x)_2Te_3$ Ternary Topological Insulators. *Nat. Commun.* **2011**, *2* (1), No. 574. DOI: 10.1038/ncomms1588
24. Cheng, R.; Ge, H.; Huang, S.; Xie, S.; Tong, Q.; Sang, H.; Yan, F.; Zhu, L.; Wang, R.; Liu, Y.; Hong, M.; Uher, C.; Zhang, Q.; Liu, W.; Tang, X. Unraveling Electronic Origins for

Boosting Thermoelectric Performance of p-Type $(Bi,Sb)_2Te_3$. *Sci. Adv.* **2024**, *10* (21), No. eadn9959. DOI: 10.1126/sciadv.adn9959

25. Plucinski, L.; Herdt, A.; Fahrendorf, S.; Bihlmayer, G.; Mussler, G.; Döring, S.; Kampmeier, J.; Matthes, F.; Bürgler, D. E.; Grützmacher, D.; Blügel, S.; Schneider, C. M. Electronic Structure, Surface Morphology, and Topologically Protected Surface States of Sb_2Te_3 Thin Films Grown on Si(111). *J. Appl. Phys.* **2013**, *113* (5), No. 053706. DOI: 10.1063/1.4789353
26. Eschbach, M.; Młyńczak, E.; Kellner, J.; Kampmeier, J.; Lanius, M.; Neumann, E.; Weyrich, C.; Gehlmann, M.; Gospodarič, P.; Döring, S.; Mussler, G.; Demarina, N.; Luysberg, M.; Bihlmayer, G.; Schäpers, T.; Plucinski, L.; Blügel, S.; Morgenstern, M.; Schneider, C. M.; Grützmacher, D. Realization of a Vertical Topological p-n Junction in Epitaxial Sb_2Te_3/Bi_2Te_3 Heterostructures. *Nat. Commun.* **2015**, *6* (1), No. 8816. DOI: 10.1038/ncomms9816
27. Novotny, V.; Meincke, P. P. M. Single Superconducting Energy Gap in Pure Niobium. *J. Low Temp. Phys.* **1975**, *18* (1), 147–157. DOI: 10.1007/BF00116976
28. Kodama, J.; Itoh, M.; Hirai, H. Superconducting Transition Temperature Versus Thickness of Nb Film on Various Substrates. *J. Appl. Phys.* **1983**, *54* (7), 4050–4054. DOI: 10.1063/1.332534
29. Gubin, A. I.; Il'in, K. S.; Vitusevich, S. A.; Siegel, M.; Klein, N. Dependence of Magnetic Penetration Depth on the Thickness of Superconducting Nb Thin Films. *Phys. Rev. B* **2005**, *72* (6), No. 064503. DOI: 10.1103/PhysRevB.72.064503
30. Song, X.; Babu, S. S.; Bai, Y.; Golubev, D. S.; Burkova, I.; Romanov, A.; Ilin, E.; Eckstein, J. N.; Bezryadin, A. Interference, Diffraction, and Diode Effects in

Superconducting Array Based on Bismuth Antimony Telluride Topological Insulator. *Commun. Phys.* **2023**, *6* (1), No. 177. DOI: 10.1038/s42005-023-01288-9

31. Zhang, H.; Ma, X.; Li, L.; Langenberg, D.; Zeng, C. G.; Miao, G. X. Two-Step Growth of High-Quality Nb/$(Bi_{0.5}Sb_{0.5})_2Te_3$/Nb Heterostructures for Topological Josephson Junctions. *J. Mater. Res.* **2018**, *33* (16), 2423–2433. DOI: 10.1557/jmr.2018.195

32. Xu, C.-Z.; Liu, Y.; Yukawa, R.; Zhang, L.-X.; Matsuda, I.; Miller, T.; Chiang, T.-C. Photoemission Circular Dichroism and Spin Polarization of the Topological Surface States in Ultrathin Bi_2Te_3 Films. *Phys. Rev. Lett.* **2015**, *115* (1), No. 016801. DOI: 10.1103/PhysRevLett.115.016801

33. Liu, Y.; Bian, G.; Miller, T.; Bissen, M.; Chiang, T.-C. Topological Limit of Ultrathin Quasi-Free-Standing Bi_2Te_3 Films Grown on Si(111). *Phys. Rev. B* **2012**, *85* (19), No. 195442. DOI: 10.1103/PhysRevB.85.195442

34. Dynes, R. C.; Narayanamurti, V.; Garno, J. P. Direct Measurement of Quasiparticle-Lifetime Broadening in a Strong-Coupled Superconductor. *Phys. Rev. Lett.* **1978**, *41* (21), 1509–1512. DOI: 10.1103/PhysRevLett.41.1509

35. Klapwijk, T. M. Proximity Effect from an Andreev Perspective. *J. Supercond.* **2004**, *17* (5), 593–611. DOI: 10.1007/s10948-004-0773-0

36. Ota, Y.; Okazaki, K.; Yamamoto, H. Q.; Yamamoto, T.; Watanabe, S.; Chen, C.; Nagao, M.; Watauchi, S.; Tanaka, I.; Takano, Y.; Shin, S. Unconventional Superconductivity in the BiS_2-Based Layered Superconductor $NdO_{0.71}F_{0.29}BiS_2$. *Phys. Rev. Lett.* **2017**, *118* (16), No. 167002. DOI: 10.1103/PhysRevLett.118.167002

37. Okazaki, K.; Ota, Y.; Kotani, Y.; Malaeb, W.; Ishida, Y.; Shimojima, T.; Kiss, T.; Watanabe, S.; Chen, C.-T.; Kihou, K.; Lee, C. H.; Iyo, A.; Eisaki, H.; Saito, T.;

Fukazawa, H.; Kohori, Y.; Hashimoto, K.; Shibauchi, T.; Matsuda, Y.; Ikeda, H.; *et al.* Octet-Line Node Structure of Superconducting Order Parameter in KFe_2As_2. *Science* **2012**, *337* (6100), 1314–1317. DOI: 10.1126/science.1222793

38. Zhong, Y.; Liu, J.; Wu, X.; Guguchia, Z.; Yin, J.-X.; Mine, A.; Li, Y.; Najafzadeh, S.; Das, D.; Mielke III, C.; Khasanov, R.; Luetkens, H.; Suzuki, T.; Liu, K.; Han, X.; Kondo, T.; Hu, J.; Shin, S.; Wang, Z.; Shi, X.; *et al.* Nodeless Electron Pairing in CsV_3Sb_5-Derived Kagome Superconductors. *Nature* **2023**, *617* (7961), 488–492. DOI: 10.1038/s41586-023-05907-x
39. Odobesko, A.; Friedrich, F.; Zhang, S.-B.; Haldar, S.; Heinze, S.; Trauzettel, B.; Bode, M. Anisotropic Vortices on Superconducting Nb(110). *Phys. Rev. B* **2020**, *102* (17), No. 174502. DOI: 10.1103/PhysRevB.102.174502
40. Rüßmann, P.; Blügel, S. Density Functional Bogoliubov-de Gennes Analysis of Superconducting Nb and Nb(110) Surfaces. *Phys. Rev. B* **2022**, *105* (12), No. 125143. DOI: 10.1103/PhysRevB.105.125143
41. Giannozzi, P.; Baroni, S.; Bonini, N.; Calandra, M.; Car, R.; Cavazzoni, C.; Ceresoli, D.; Chiarotti, G. L.; Cococcioni, M.; Dabo, I.; Dal Corso, A.; de Gironcoli, S.; Fabris, S.; Fratesi, G.; Gebauer, R.; Gerstmann, U.; Gougoussis, C.; Kokalj, A.; Lazzeri, M.; Martin-Samos, L.; *et al.* QUANTUM ESPRESSO: A Modular and Open-Source Software Project for Quantum Simulations of Materials. *J. Phys.: Condens. Matter* **2009**, *21* (39), No. 395502. DOI: 10.1088/0953-8984/21/39/395502
42. Perdew, J. P.; Burke, K.; Ernzerhof, M. Generalized Gradient Approximation Made Simple. *Phys. Rev. Lett.* **1996**, *77* (18), 3865–3868. DOI: 10.1103/PhysRevLett.77.3865

43. Blöchl, P. E. Projector Augmented-Wave Method. *Phys. Rev. B* **1994**, *50* (24), 17953–17979. DOI: 10.1103/PhysRevB.50.17953

44. Grimme, S.; Antony, J.; Ehrlich, S.; Krieg, H. A Consistent and Accurate *Ab Initio* Parametrization of Density Functional Dispersion Correction (DFT-D) for the 94 Elements H-Pu. *J. Chem. Phys.* **2010**, *132* (15), No. 154104. DOI: 10.1063/1.3382344

45. Monkhorst, H. J.; Pack, J. D. Special Points for Brillouin-Zone Integrations. *Phys. Rev. B* **1976**, *13* (12), 5188–5192. DOI: 10.1103/PhysRevB.13.5188